DOI: 10.30632/SPWLA-2022-0095

BHI LOGS AND ML AUTOMATED PRE-SALT CARBONATE: TEXTURE RECOGNITION AND PETROPHYSICAL PROPERTIES PROPAGATION USING IMAGE LOG, CORE IMAGES AND POROSITY-PERMEABILITY FROM PLUGS

Barbara Quediman, Enrique Estrada, Radompon Sungkorn & Jonas Toelke, Halliburton

This paper was prepared for presentation at the SPWLA 63rd Annual Logging Symposium held in Stavanger, Norway, June 10-15, 2022.

ABSTRACT

Identifying depositional facies and diagenetic modifications from BHI logs in sections without core is challenging due to heterogeneities in fabric of the carbonaceous rock, which are below the resolution of the BHI logs in these complex reservoirs. This is mainly due to different diagenetic processes resulting in different types of reservoir rocks (RRTs) with different petrophysical properties in the same geological facies. This work describes an innovative new workflow that uses a deep learning model to identify heterogeneities of fabric (textures) in complex carbonate reservoirs in sections without core; as input we use conventional (gamma ray, density, neutron, sonic), NMR, BHI (acoustic imaging) logs, core CT images and physical porosity and permeability measurements from plugs. This new workflow combines supervised deep learning and unsupervised machine learning methods, consisting of four steps: (1) Identification of textures in Core CT (2) Calibration of features of BHI logs in core section (3) Training a deep learning model with cropped images from BHI logs to extract texture curves (4) train a machine learning regression model with texture curves, WL logs and plug porosity and permeability values to propagate prediction of textures, porosity and permeability along the well. The texture curves generated by the ML model are in good match with the recognized core section textures (CT Images). The results show that the NMR Total Porosity has a good correlation with the porosity predicted by the regression model. In addition, the petrophysical data from plugs measured in the laboratory show a good match with the porosity and permeability predicted in the core zone. In the non-core zone, the predicted textures by the ML model relate to the heterogeneities of the carbonaceous rock fabric and the propagation of the petrophysical properties have good correlation with the predicted textures. In some cases, vuggy porosity combined with fractures do not allow correct porosity measurement with NMR or density tools due to the sensitivity of these tools to poor borehole conditions. In these cases, the NMR presents a fast relaxation of the T2 distribution due to the heterogeneity of these carbonaceous fabric and therefore the porosity and permeability measurements will be affected. The ML model uses CT Textures to calibrate BHI Crops in the core section zone and NMR and Basic logs as input, improving the recognition of the textural heterogeneities and refine the traditional Rock typing of these complex Pre-Salt carbonate reservoirs.

INTRODUCTION

The recent discovery of giant pre-salt lacustrine carbonate reservoirs in the south Atlantic Cretaceous rift system of Brazil has sparked a great deal of interest in Carbonates formed and deposited in continental environments. The challenges in these reservoirs due to intense diagenesis results in large vertical and lateral variations in the quality of the rock (permeability and porosity). This can be observed as drilling shows a low rate of penetration in hard and abrasive carbonate rock mixed with silica and igneous rock intercalation, further complicated by the presence of natural and tensile fractures, breakouts and washouts (cavern and caves) generating severe loss of fluid due to significant control over the diagenetic processes (Estrada *et al.,2019*).

There have been articles published describing these Pre-salt deposits and diagenetic modifications (Terra *et al*., 2010; Muniz and Bosence, 2015; Wright and Barnett, 2015; Wright and Barnett, 2017; Herlinger *et al*., 2017, Lima and De Ros, 2019; Wright and Barnett, 2017, 2019, Ceraldi & Green, 2016, Mercedes Martin et al., 2019, etc.).

Figure 1 shows the stratigraphy of the Barra Velha Formation (Moreira *et al., 2007*) that starts with the deposition of Camboriú Formation basalts as a response to the first signs of the Gondwana breakup. During the early rift stages, sandstones, siltstones, and shales of talc-stevensitic composition were deposited in a lacustrine environment and represent the Piçarras Formation of Barremian age. From the Neo-barremian until the Eo-

Aptian, high energy bivalve grainstones and rudstones (coquinas) of the Itapema Formation were deposited. The Barra Velha Formation carbonates (stromatolites, grainstones and packstone) were deposited in the Aptian, during the post rift stage characterized by the transition from continental to a shallow marine setting and by the end of the Aptian, after the establishment of an open marine setting, a thick salt sequence from the Ariri Formation.

Aptian pre-salt reservoirs, in Barra Velha Formation (BVF), consist of layers, centimeters to decimeters thick, of lacustrine carbonates illustrated in Figure 2 (Petersohn *et al*. 2013). The predominant sedimentary facies are chemical, microbial, and hydrothermal precipitation products.

The reservoirs contain intervals of fascicular calcite and spherulites aggregates precipitates and laminated strata made of syngenetic magnesian clay minerals (e.g., Tosca and Wright, 2015; Wright and Barnett, 2015; Wright and Tosca, 2016; Herlinger Jr. and De Ros., 2017; Lima and De Ros., 2019, Dias da Silva, M. et al., 2021, Rammani, C., et al., 2020). Also, in some instances, present dolomitization, silicification, cementation, dissolution, and/or recrystallization were promoted in association with tectonic and hydraulic fracturing (Herlinger Jr. et al., 2017; Poros et al., 2017; Vieira de Luca et al., 2017) and many authors, interpreted that these alterations may have been related to processes occurring during burial and to the flow of hydrothermal fluids (e.g., Alvarenga et al., 2016; Vieira de Luca et al., 2017, Lima and De Ros., 2019)

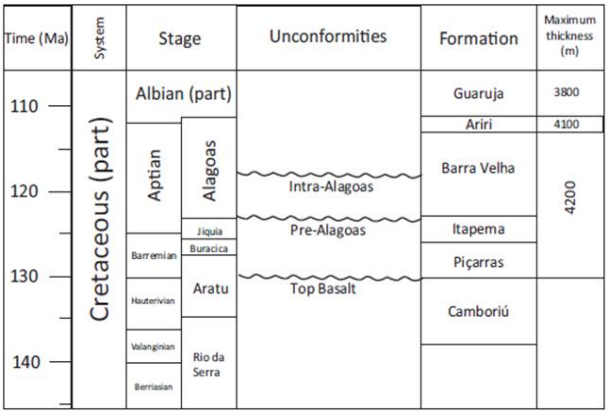

Figure 1. Stratigraphy of the Barra Velha Formation (Moreira et al. 2007).

Figure 3 shows facies for the Barra Velha Formation which have been documented by Barnett *et al*., 2021, Wright and Barnett, (2015), where they describe 5 main facies and different lithofacies types for each one: 1-Calcimudstones (Lithotypes 1A, 1B 1C), 2-Spherulites (Lithotypes 2A, 2B 2C, 2D), 3-Crystal Shrubs (Lithotypes 3A, 3B, 3C, 3D), 4- Microbiolites (Lithotypes 4A, 4B, 4C, 4D) and 5- Grainstone/Rudstone. (5A). Barnett *et al*. 2021 in Lula field describes on the top, had more abundant Shrub in the succession Shrub/Spherulite than at the base of Barra Velha formation, we can observe similar behavior in our study.

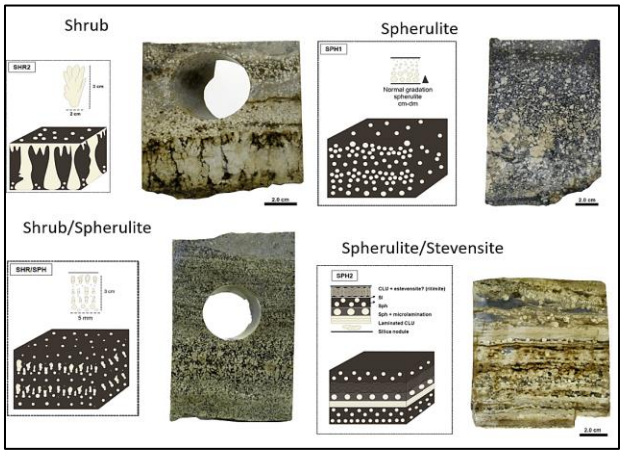

Figure 2. Complex fabric of pre salt carbonate (Petersohn et al., 2013)

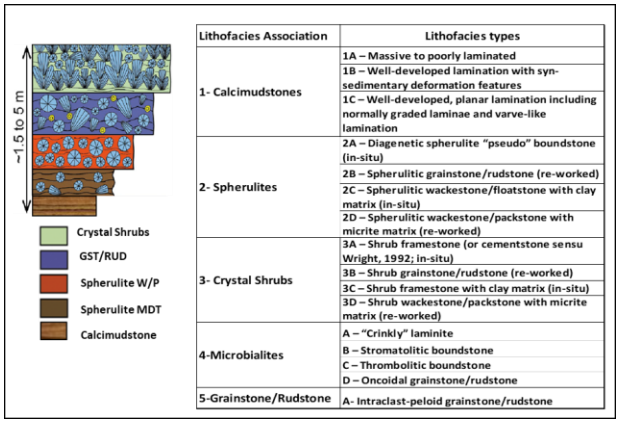

Figure 3. Facies and Lithofacies types (Barnett, 2021, Modified from Martin, et al., 2019)

The evaluation of borehole images in carbonate reservoirs from different depositional environments with a variety of diagenetic histories indicates that this technique provides valuable information on porosity heterogeneities. Electrical and acoustic images, which have high resolution and provide three-dimensional data, have greatly improved facies identification and interpretation, particularly when integrated with core data.

Muniz & Bosence (2015) for the Macabu formation in the SE of Campos Basin, described the

characterization of facies, image logs facies and cyclicity in lacustrine carbonates. The karst petrophysical properties have been a challenge, mostly because of the lack of reliable information about the mega and giga pore network, such as large vugs, caves, conduits and enlarged fractures (Menezes *et al.*, 2016, 2019), therefore these types of reservoirs have variations since as severe loss of fluids, natural and tensile fracture, breakout and washout cavern and cave are very often related to low rate of penetration and hard abrasive carbonate; silica and igneous rock intercalations. Large individual pores, fractures, and cavities are often directly visible on these images, although microscopic pores are below the resolution of the technique.

Pore characterization (BVM, BVI, CBW) are commonly performed by magnetic resonance (NMR) logs in pre-salt wells. However, NMR has limitations related to pore sizes up to 100 microns and the assumption of a lack of diffusion effects. If diffusion effects are strong and the pore size is greater than 100 microns, the t2 distribution is no longer considered representative of the pore body distribution. Predicting pore types in the logarithmic domain and coreless intervals can be very challenging without a strong link to geological trends (Skalinski & Kenter, *2014*, Sung *et al.*, 2013). On the other hand, the characterization of micropores with NMR is another of the limitations that we have in these complex pre-salt rocks. Additionally, the structures of the shrubs show a variety of textures of these shrubs/spherulites on a decimetric scale of microscopic pores (e.g., morphologies, size, sizing, and packing), as shown in the complex pore networks described by Erthal, M. (2018). The characterization of carbonate textures, structure, pore types, and porosity distribution from borehole image logs only, are not representative due to microscopic pores which are below the resolution of the borehole images This is due to the complexity of the heterogeneities within these pre-salt carbonate facies which generate different RRTs with petrophysical properties in the same facies. Bize (et al., 2016) use artificial intelligence and BHI Logs to predict geological facies in pre salt carbonate.

The evaluation of borehole image logs in conjunction with core tomographic images and the combination of artificial intelligence in this study; indicates that this technique provides new and valuable information for the evaluation of porosity heterogeneities. High resolution core tomographic images allow us to evaluate and characterize the complex pore network related to the different textures of these pre-salt carbonates; allowing to calibrate the geological features in the borehole image with the tomographic image in the core section; to be the input of the deep machine learning model.

METHODOLOGY

This new workflow uses a combination of supervised and unsupervised deep learning methods from conventional logs and special BHI and NMR logs, as well as high-resolution core tomographic images (CT) and physical data of the porosity and permeability of core plugs.

The supervised method is vital to generate the basis of a learned model from previously grouped training data. The unsupervised methods allow us to statistically identify patterns in this data and make a prediction to propagate throughout the well.

For this work, the triplet loss function was used for machine learning algorithms. This function is designed to optimize a neural network that produces embeddings used for comparison, where a reference input (Anchor) is compared with a matching input (Positive) and a non-matching input (Negative). The method works as follows; the distance from the anchor or reference to the positive input is minimized when the images are similar and the distance from the anchor to the negative input is maximized when the images are different. The choice of the best parameters that contribute significantly to the robustness of the propagation model is done through the training-validation process.

Data Preparation: Before starting this workflow the data from conventional well logs such as GR, DEN, RES, NEU, DTC, DTS and special logs from Borehole Image Logs (BHI) and NMR (Acoustic Imaging); are subject to strict quality control; depth shift, missing data and anomalous values, as well as porosity and permeability data from plugs and Core Tomography (orientation of core CT Image sections and depth matching), represent a very important step in achieving model accuracy of training.

The workflow consists of four compound and sequential supervised and unsupervised steps. Following is a brief description of each of the workflow step:

Step 1: Texture identification and description from Core CT Images- (Method Supervised)

Using high-resolution core tomography images (0.3mm), the predominant textures in the core sections were identified and described manually. Eight textures

were identified (Figure 4) which are listed below:

Texture 1: Massive-Tight carbonates deposits of fine to very fine grain size without porosity.

Texture 2: Carbonate breccia formed by chaotic angular fragments of microbial carbonates (Broken Shrubs) with random orientation.

Texture 3: Structureless (reworked-Shrubs-Spherulite) small grain size carbonates deposits, predominating very small black hole (micro interparticle porosity).

Texture 4: Carbonates laminated deposits with alternating layers of fine to very fine grain sizes.

Texture 5: Laminated carbonates deposits with alternating thicker and finer layers made up of two types of granulometries, coarser-predominantly more porous and finer-less porous. (Shrubs/Spherulite)

Texture 6: Structureless (reworked-Shrubs- Spherulite) medium grain size deposits, predominating medium black hole (meso interparticle porosity).

Texture 7: Structureless (reworked- Shrubs -Spherulite) large grain size deposits, predominating big black hole (macro interparticle porosity).

Texture 8: Laminated deposits comprising layers of individual shrubs (microbial influence) which branch as they grow upwards, forming convex structures.

Step 2: Calibration BHI Facies – Core section- (Method Supervised)

This step comprises the calibration of BHI facies in the core section with the textures described in tomography images of the core in step 1. The criteria used to interpret BHI facies are patterns in color variation, images of texture, sedimentary structures and diagenetic structures. Nine BHI facies (BHI-1 to BHI-9) were interpreted. The description of these BHI facies (Figure 5) are detailed below:

BHI-F1: This facie is characterized by very thin flat layers interspersed with more resistive layers (bright) and a high and uniform acoustic amplitude (bright).

BHI-F2: This facie is characterized by a pattern of broken clasts or blocks with a random pattern with high resistivity (bright) and high and low acoustic amplitude (dark).

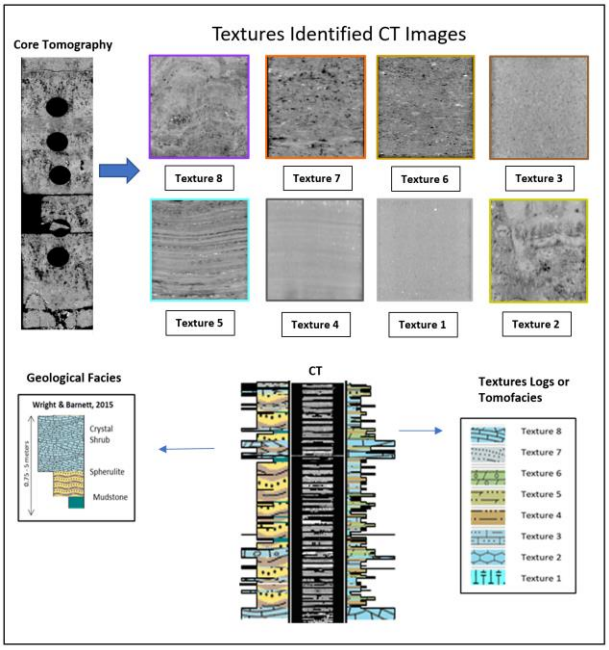

Figure 4. Step 1-Textures Identification and Description from Core CT Images - (Method Supervised). Texture 1: Massive-tight Carbonates. Texture 2: Carbonates breccia fragments. Texture 3: Reworked-Shrubs-Spherulites, micro-interparticle porosity. Texture 4: Laminated Fine. Texture 5: Laminated porous. Texture 6: Reworked-Shrubs-Spherulites, meso-interparticle porosity. Texture 7: Reworked-Shrubs-Spherulites, macro-interparticle porosity. Texture 8: Laminated deposits of individual Shrubs.

BHI-F3: This facie is characterized by a mottled pattern that reflects a fine-grained texture with very small cavities, high resistivity (bright) and high acoustic amplitude (bright).

BHI-F4: This facie is characterized by thin layers interbedded with layers more conductive (dark) and high acoustic amplitude (bright).

BHI-F5: This facie is characterized by alternating thin-porous layers of high resistivity (bright) and more conductive (dark) and low acoustic amplitude (dark).

BHI-F6: This facie is characterized by a mottled pattern that reflects a grainy texture with scattered medium cavities of more resistivity (bright) and low acoustic amplitude (dark) interpreted as possibly mouldic, intergranular or vuggy porosity.

BHI-F7: This facie is characterized by a mottled pattern that reflects a grainy texture with scattered medium to large cavities of more resistivity (bright) and low acoustic amplitude (dark), interpreted as possible possibly

mouldic, intergranular or vuggy porosity.

BHI-F8: This facie is characterized by dome-shaped or convex layers (Microbial-Shrubs) alternating high resistivity (bright) and more conductive (dark) and in some cases with medium to large dark cavities alternating in the layer low acoustic amplitude (dark), interpreted as vugular porosity.

BHI-F9: This facie is characterized by large to very large cavities of high resistivity (bright) and low acoustic amplitude (dark) randomly dispersed and the presence of natural fractures of high resistivity (bright) and low acoustic amplitude (dark).

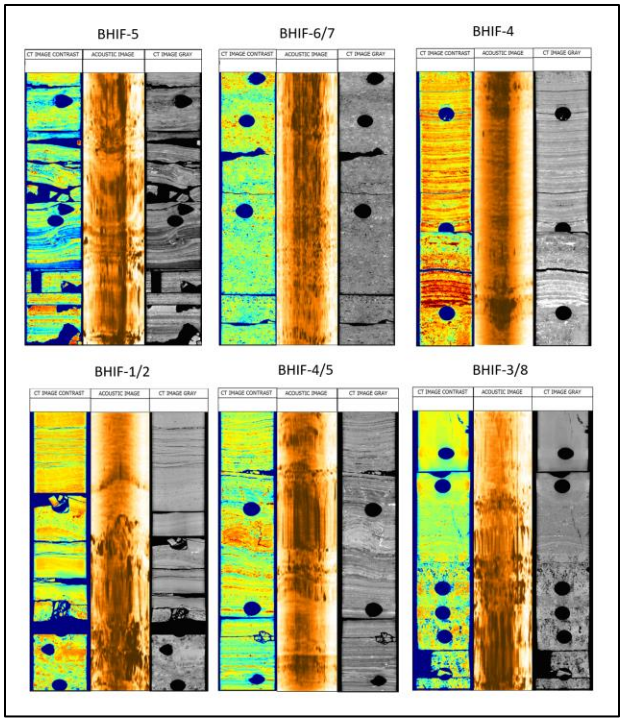

Figure 5. Step 2- Calibration BHI Facies. BHIF-1: Thin flat layer. BHIF-2: Breccia (Broken clast or blocks). BHIF-3: Mottled pattern. BHIF-4: Thin layers. BHIF-5: Thin-porous layers. BHIF-6: Mottled pattern medium cavities. BHIF-7: Mottled pattern medium to large cavities. BHIF-8: Shrub or convex layers.

Step 3: BHI Crops -Grouping-Textures Curves - (Method Supervised-Unsupervised)

After the calibration of the BHI Facies in Step 2 in the core zone; using software, a plurality of crops or patches were generated from the borehole image logs (Acoustic images), one every 0.15 m to generate a working dataset. Then the dimensionality of that dataset is reduced to 20% of the total data generated; where each crop is large enough to capture one type of texture or geological feature. The textural grouping was done manually (SME Geologist - Supervised Method), generating a grouped dataset that is the input of the machine learning training model. To carry out the deep learning training, the triplet loss function was used, combining the data in an embedding space environment using a statistical method (t-SNE) to visualize each point in a three-dimensional space preserving the embeddings, where each data point is represented by a number 1, 2, 3 generating texture curves as output. (Figure.6).

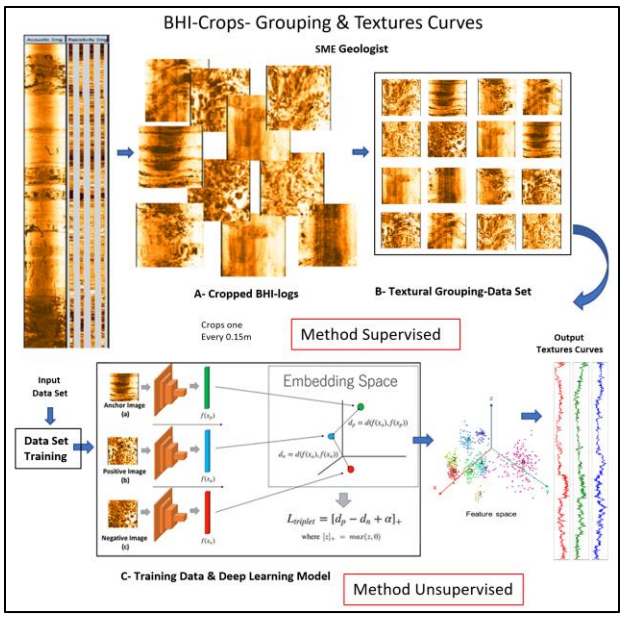

Figure 6. Step 3 BHI Crops –Grouping-Textures Curves – (Method Supervised-Unsupervised). A-Cropped BHI logs, using software to generate plurality one every 0.15m. B- Textural Grouping Data Set, generated manually by SME Geologist. C-Training Data & Deep Learning Model, using Triplet-Loss algorithm, to generated Textures Curves.

Step4: Deep-learning model & PPP- (Method Unsupervised)

The texture curves (1, 2, 3) obtained in Step 3 from the triplet loss model are combined with basic and special well logs as well as physical measurements of porosity (PHI) and permeability (K) in core plugs (minimum data required 3-5 (K-PHI) per texture. Then applying a regression to extract the relationship/model the input variable (well logs and textures curves) and the output (porosity and permeability), to propagate a prediction of textures, porosity, and permeability along the well. (Figure.7).

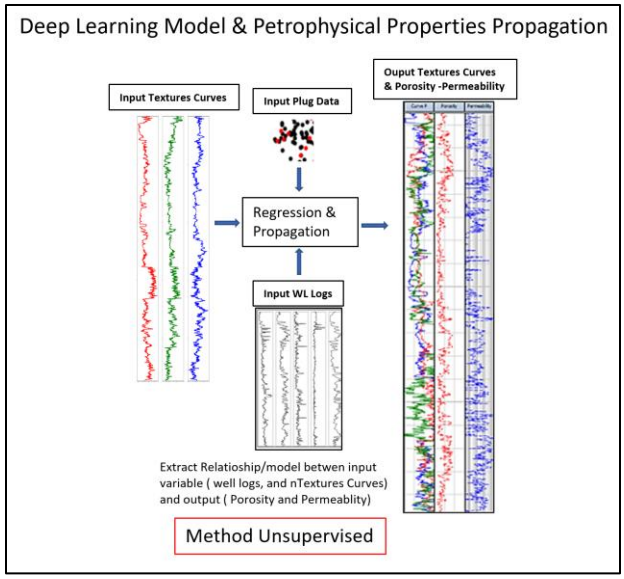

Figure 7. Step 4 Deep learning Model & Petrophysical Properties Propagation (Method Unsupervised)-

RESULTS

The results shown in Figure 8A present the textures predicted by the ML model using BHI Crops, NMR and basic logs as input, improving recognition of textural heterogeneities from these complex pre-salt carbonate reservoirs. Where the NMR Total Porosity (track 5), which has a good correlation with the porosity predicted by the regression model, shows a good fit with the predicted textures (track 9) throughout this interval. The zones of medium to high NMR porosity values coincide with textures 5-8 and the zones of low values with textures 1-4.

Figure 8B represents a red rectangle zoom of figure 8A of the core zone, the Facies (facies associations of shrub, spherulites and calci-mudstones) are observed in the first track. Track 2 CT illustrates the tomographic image of the slabbed core and the black holes in the plugged areas. The textures described in the tomography can be observed in track 3 and from 4 to track 7 the predicted ML model. The predicted textures in (track 5) show a good match with the main textures of the core section. The petrophysical data of the plugs measured in the laboratory were used to train the model in the core zone using 70% of the data and leaving 30% for validation, as seen in tracks 6 and 7, the predicted curves show a fit with petrophysical plugs.

Figure 8C shows the result of the lower part of the well, where a new texture (9) predicted by the ML model is shown in the upper part, which was not recognized in the core tomography analysis.

Figure 8D shows a zoom in the red color rectangle where the presence of vugs can be seen in the acoustic image (dark brown color), showing a highly connected area with high porosity and permeability. The NMR shows a rapid relaxation of the T2 distribution due to the heterogeneity of these carbonaceous rocks and therefore the porosity measurements will be affected, showing a high value of BVI, which is something very common in pre-salt reservoirs. Cave porosities combined with fractures do not allow correct porosity measurement with NMR or density tools due to the sensitivity of these tools to poor well conditions. In tracks 11 and 12 from (figure 8C), the ML model it has been possible to predict porosities and permeabilities in these areas of great production of hydrocarbons. This texture was found several times throughout the well showing the same characteristics with the Imaging and NMR logs.

The Winland r35 plot shows results about this methodology, although the diagenetic modifications severely affect each of these textures. As we know in pre salt carbonate the textural variations are very large due to the different fabrics formed by the diagenetic modifications. In the PhiT/K Winland plot (Figure 8E) we can see the distribution of some of these textures that may have high connectivity with high porosity and permeability and in other cases present medium to low values of porosity and permeability. This is because, as described in (Figure 3) above, these spherulite facies could correspond to 2A, 2B, 2C, 2D (texture 5). The same goes for texture 8 (purple) which shows variations of Shrub 3A, 3B, 3C 3D. The textures that are enclosed in a circle to the right represent the areas of preferential dissolution (Diagenetic zone) and to the left areas preferentially susceptible to micro cracks or micro fractures that can connect small pores.

Without a doubt, the diagenetic modifications in textures 5-8 play a more important role than in textures 1-4. Where, on the one hand, we know that the upper part of Barra Velha Formation is more subject to dissolution when gases ascend through faults during oil migration generating secondary porosities, and that they are interrupted when the Ariri (Salt) formation is reached. The distribution of secondary porosity will essentially be dominated by the distribution of porous textures along these upper Barra Velha intervals. Fine and tight textures (common to the bottom of Barra Velha Formation) will not have a large increase in secondary porosity, as will textures with intergranular porosity and with cavities such as Shrubs and spherulites. It should be noted that we can

find Shrubs and spherulites with low porosities and permeabilities due to the cementation of their pores or in some cases to the presence of Mg-clay minerals (Dias da Silva, M. *et al., 2021*, Rammani, C., *et al., 2020*), this type of variation in lithofacies types 3C and 3D is shown in detail in Figure 3 (Barnett, et al., 2021).

We can say that in (Figure 8F), all the previous textures are susceptible to being diagenetically modified and can be summarized in a general way, of course there are areas with high diagenetic modifications and areas more prone to fracture, as shown in the Plot Winland r35. The distribution of the RRT following the traditional methodology could make us omit a significant number of carbonate fabrics that are only visible in thin section or in electron microscopy, as can be described in Figure 3 (Lithofacies types). Since we know that the textures obtained from the core tomography images allow us to recognize at least some of the characteristics of the lithofacies types, for that, the experience of the SME Geologist is vital to recognize these textures (supervised). Once we have adjusted the BHI textures at the core level then we can use artificial intelligence such as deep learning to be able to extend them to the whole well.

Figure 9 shows the results integrated into a large graph where, from borehole images and the use of artificial intelligence (Machine learning) can be applied to predict texture variations in carbonate rocks throughout the well. The prediction of these textures throughout the well agrees well with the porosity and permeability calculated from the ML-PPP, as well as with the NMR porosity. On the other hand, one of the biggest problems mentioned above in the pre-salt is due to the effect of the porosity measurement in the presence of caverns and fractured zones, where the relaxation of t2 is very fast, reaching only BVI values, with which, the measurement of porosity is difficult and affects the calculation of permeability (Figure 8D). In this case, from borehole images, a new texture (texture 9) was predicted for zones with vugs and highly connected fractures, with good porosity and permeability, being very important in these zones of productive interest.

CONCLUSION

Highly connected lithofacies such as Shrubs (3A-3B) and Spherulites (2B), generally represented by textures 5-9, will be found in the zone of high diagenetic modifications, considerably increasing their porosity and permeability in upper Barra Velha Formation. However, the fine lithofacies will have greater modifications in the lower part of Barra Velha Formation due to their fracturing, showing vertical connections (plug) in the fine and tight textures (textures 1-4). In the lower zone of Barra Velha, fine, tight laminated textures are very abundant, frequently intercalated with Shrub, which are what contribute to the porosity and permeability in these zones. The predicting of textures along of well from BHI allow us, refined our rock typing and improvement our petrophysical analysis, due more adjustment of porosity and permeability with these textures.

ACKNOWLEGDE

This work was conducted by Halliburton Produtos Ltda (HPL) in association with the ongoing Project registered under ANP number 21004-7 as “Pesquisas avançadas em análise digital de rocha para carbonatos do pré-sal: Integrando rocha digital, análise de laboratório, inteligência artificial, dados de poços e sísmica em diferentes escalas para aplicação em modelagem de reservatórios” (HPL/Shell Brazil/ANP) funded by Shell Brazil R&D program, under the ANP R&D levy as "Compromisso de Investimentos com Pesquisa e Desenvolvimento". The authors would like to thank to Chief Robert Gales, Dr. Luis Quintero and Champion Peter Barrett for their contributions, their incentive and technical advice.

SAMPLE NOMENCLATURE

Abbreviations

GR = Gamma Ray
RT = True Resistivity
LLD=Deep Resistivity
LLS=Shallow Resistivity
DEN = Density
NEU= Neutron
DTC = Sonic Compressional
DTS = Sonic Shear
BHI = Borehole Image log
BHI-F=Borehole Image Facies
CT = Core Tomography Image
DAL= Aluminum weight fraction
DSUL= Sulfurs weight fraction
DSI=Silica weight fraction
DCA= Calcium weight fraction
DMG=Magnesium weight fraction
DFE=Iron weight fraction
TH = Thorium
K = Potassium
U = Uranium
MSIGTA=Total porosity
MPHITA=Effective porosity
MFFITA=Free Fluid porosity

NMR = Nuclear Magnetic Resonance
BVI=Bulk Volume Irreducible
BVM= Bulk Volume Mobil
ML=Machine Learning Model
PPP=Petrophysical Properties Propagation

REFERENCES

Alvarenga, R.S., Iacopini, D., Kuchle, J., Scherer, C.M.S., Goldberg, K., 2016. Seismic characteristics and distribution of hydrothermal vent complexes in the Cretaceous offshore rift section of the Campos Basin, offshore Brazil. Marine and Petroleum Geology 74, 12–25

Barnett A. J., Obermaier M., Amthor J., Sharafodin M, Bolton M., Clarke D., and Camara R., 2021, Origin and Significance of Thick Carbonate Grainstone Packages in Nonmarine Successions: A Case Study from the Barra Velha Formation, Santos Basin, Brazil, *in Marcio R. Mello, Pinar O. Yilmaz, and Barry J. Katz, eds*, The Supergiant Lower Cretaceous pre-salt petroleum systems of the Santos Basin, Brazil: AAPG Memoir124, p. 155-174. DOI: 10.1306/13722318MSB.6.1853.

Bize-Forest N., Lima L., Baines V, Boyd A., Abbots F. and A. Barnett, 2018, Using Machine- Learning for Depositional Facies Prediction in a Complex Carbonate Reservoir. SPWLA 59 th Annual Logging Symposium, June 2-6, 2018.

Da Silva, M.D.; Gomes, M.E.B.; Mexias, A.S.; Pozo, M.; Drago, S.M.; Célia, R.S.; Silva, L.A.C.; Netto,P.; Gomes, L.B.; Porcher, C.C.; Dani, R.; Driemeyer, D. ; Rammani, C.; and J. F. Santos. Mineralogical Study of Levels with Magnesian Clay Minerals in the Santos Basin, Aptian Pre-Salt Brazil. Minerals 2021, 11, 970. https://doi.org/10.3390/min11090970

Erthal Marques, M., 2018, Travertine Shrub Structures: Origin, diagenetic modifications and petrophysical characteristics-Tivoli case (Central Italy). Dissertation presented in partial fulfillment of the requirements for the degree of Doctor of Science (geology). ©2017 KU Leuven, Science, Engineering & Technology Arenberg Doctoraatsschool, W. De Croylann, 3001 Heverlee, België).

Estrada, E., Lima A. & M. Celestino. The Construction of Predictive Model to Reductions in Time and Cost of the Appraisal & Exploratory Well. AAPG GTW 2019 Brazil. https://www.searchanddiscovery.com/pdfz/documents/2020/42432estrada/ndx_estrada.pdf.html

Estrada E, Quediman B, March R, Drexler S, Siqueira M and J. Toelke. Digital Rock application to refined geological and reservoirs models: Integrating core and plug CT images & Image Logs for texture analysis in pre salt reservoir, Brazil. Extended Abstract IRIS 2020.

Herlinger Jr R, Zambonato E, & L. De Ros, 2017. Influence of diagenesis on the quality of lower cretaceous Pre-Salt lacustrine carbonate reservoirs from northern Campos Basin, offshore Brazil. Journal of Sedimentary Research 87, 1285–1313.

Lima, B., & L. De Ros, 2019. Deposition, diagenetic and hydrothermal processes in the Aptian Pre-Salt Lacustrine carbonate reservoirs of the northern Campos Basin, offshore Brazil. Sedimentary Geology 383 (2019) 55–81

Martin, R. M., Ayora C., Tritla J, Sanchez Roman, M., 2019, The hydrochemical evolution of alkaline volcanic lakes: a model to understand the South Atlantic Pre-salt mineral assemblages, Earth- Science Reviews https://doi.org/ 10.1016/j.earscirev.2019.102938

Menezes de Jesus, C., Martins Compan A. L., and R. Surmas, 2016, Permeability Estimation Using Ultrasonic Borehole Image Logs in Dual-Porosity Carbonate Reservoirs. Petrophysics, Vol. 57, NO.6 (December 2016), Page 620-637, 18 Figures.

Muniz, M.C., Bosence, D.W.J., 2015. Pre-Salt microbialites from the Campos Basin (Offshore Brazil): image log facies, facies model and cyclicity in lacustrine carbonates. *In: Bosence, D.W.J., Gibbons, K.A., LeHeron, D.P., Morgan, W.A., Pritchard, T., Vining, B.A. (Eds.),* Microbial Carbonates in Space and Time: Implications for Global Exploration and Production. Geological Society, London, Special Publications vol. 418, pp. 221–242.

Moreira, J. L. P.; Madeira C. V.; Gil J. A.; and M. A. P. Machado, 2007, Bacia de Santos: Boletim de Geociências da Petrobras, v. 15, no. 2, p. 531–550.

Petersohn, E. and Abelha, M. 2013, Libra Geological Assessment. Bidding Rounds Overview ANP.

Ramina, C. Santos, J.F.; Parizek-Silva, Y.; Madrucci. V.; Araújo, C.; Vasquez. G.; Morschbacher, M.; Bonzanini. L.A.; Viana, S.; 1, Souza, R.; Alves, D. and S. M. Anjos, 2020. Magnesian Clay Minerals in Brazilian Pre-salt Province. AAPG/SEG Image, Denver, Colorado.

Sabato Ceraldi, T. and D. Green, 2016, Evolution of the South Atlantic lacustrine deposits in response to Early Cretaceous rifting, subsidence, and lake hydrology. Article in Geological Society London Special Publications. June 2016. DOI:10.1144/SP438.10

Skalinski Mark, Kenter Jeroen, 2014, Carbonate petrophysical rock typing: integrating geological attributes and petrophysical properties while linking with dynamic behaviour. *In Agar, S.M. & Geiger, S. (eds)* Fundamental Controls on Fluid Flow in Carbonates. Geological Society, London, Special Publications, 406, http://dx.doi.org/10.1144/SP406.6

Sung, R.R., Clerke, E. A., Buiting, J.J. & A. T. Ettajer, 2013. Integrated geology, sedimentology and petrophysics application technology for multi- modal carbonate reservoirs. (IPTC paper 16988,) Paper presented at the IPTC International Conference, Beijing, China, 26-28 March 2013.

Sungkorn, R and Toelke, J, Method, and system to analyze Geologic Formation Properties, 2020, Patent Pub. No.: US 2020/0225177A1.

Terra, G.J.S., Spadini, A.R., Franca, A.B., Sombra, C.L., Zambonato, E.E., Juschaks, L.C. da S., Arienti, L.M., Erthal, M.M., Blauth, M., Franco, M.P., Matsua, N.S., Da Silva, N.G.C., Junior, P.A.M., D'Avila, R.S.F., de Souza, R.S., Tonietto, S.N., dos Anjos, S.M.C., Compinho, V.S., Winter, W.R., 2009. Classificação de rochas carbonaticas aplicável as bacias sedimentares brasileiras. Boletim de Geociencias: Petrobras, Rio de Janeiro.

Tosca N. & V. P. Wright, 2015 Diagenetic pathways linked to labile Mg-clays in lacustrine carbonate reservoirs: a model for the origin of secondary porosity in the Cretaceous pre-salt Barra Velha Formation, offshore Brazil. *In Armitage, P. J., Butcher, A. R., Churchill, J. M., Csoma, A. E., Hollis, C., Lander, R. H., Omma, J. E. & Worden, R. H. (eds)* Reservoir Quality of Clastic and Carbonate Rocks: Analysis, Modelling and Prediction. Geological Society, London, Special Publications, 435, http://doi.org/ 10.1144/SP435.1o 18, 9–29.

Vieira de Luca, P.H., Matias, H., Carballo, J., Sineva, D., Pimentel, G.A., Tritlla, J., Esteban, M.,Loma, R., Alonso, J.L.A., Jiménez, R.P., Pontet, M., Martinez, P.B., Vega, V., 2017. Breaking barriers and paradigms in presalt exploration: The Pão de Açúcar discovery (offshore Brazil*). In: Merrill, R.K., Sternbach, C.A. (Eds.), Giant Fields of the Decade 2000–2010.* American Association of Petroleum Geologists, USA, Memoir vol. 113,pp. 177–194

Wright V.P., and Barnett A. J., 2015, An abiotic model for the Development of textures in some South Atlantic early Cretaceous lacustrine carbonates, *in D. W. J. Bosence, K. A. Gibbons, D. P. Le Heron, W. A. Morgan, T. Pritchard, and B. A. Vining, eds.*, Microbial Carbonates in Space and Time: Implications for Global Exploration and Production: Geological Society of London Special Publication 418, p. 209-219.

Wright V.P., and Barnett A. J., 2017, Critically evaluating the current depositional models for the pre-salt Barra Velha Formation, offshore Brazil: AAPG Search and Discovery, Article #51439, Keynote Address given at AAPG/SEG International Conference and Exhibition, London, England, October, p.15-18, Digital Abstract, accessed November 17, 2020, http:// w w w. searchanddiscovery.com/pdfz/abstracts/pdf/2017/90310aapg/abstracts/ndx_wright.pdf.html.

Wright, V.P., Tosca, N.J., 2016. Geochemical model for the formation of the Pre-Salt reservoirs, Santos Basin, Brazil: implications for understanding reservoir distribution. Search and Discovery Article #51304. Adapted from oral presentation given at AAPG Annual Convention & Exhibition, Calgary, Alberta, Canada, June 19–22, 2016.

ABOUT THE AUTHORS

Barbara Quediman MSc. She is Principal Geologist Specialist Image Logs Ingrain-Halliburton Technology Center Brazil. Before she was working in Baker Hughes for Iraq & UAE Geomarket and Mexico Geomarket as Specialist Images Logs. She was begun her carrier in Repsol-YPF as Reservoir Geologist. She has in 2006 MSc. degree in Geomaterieux-Eaux, Poitier's University, France and in 2009 "Oil Gas Formation Evaluation Specialized" in the S.J.B. Patagonia National University.

Enrique Estrada PhD Actually, Regional Integrated Well Intervention Lead Producent Enhanced. Awarded "Formation Evaluation Excellent" SPE Brazil 2017. He joined Halliburton in 2015 for working as Carbonate Advisor in Libra Field Integrated Project, Brazil. Before was working at Baker Hughes in different positions: Team Leader Formation Evaluation Middle East Region, Geoscience Manager Mexico, Geology Coordinator for Latin America. Doctorated in Geology in 1998 Oviedo's University, Spain and post doctorated in 2006 Poitier's University, France.

Radompon Sungkon PhD. Chief Data Scientist at Halliburton as Leading team to develop machine learning-based applications graphical user interface and deployment. He has different positions as Principal Scientist in Machine Learning, Deep Learning and Applications at Ingrain. He has 2007 MCs Leibniz Universität Hannover; 2011 Doctorated Technische Universität Graz and 2013 Postdoctoral Fellow Alberta's University in the multiphase numerical simulation group in Chemical and Materials Engineering.

Jonas Toelke PhD. Product Development Manager for Ingrain Halliburton until February 2022. Implementation of a multi-scale digital rock physics workflow and leading development at Ingrain since 2012. He held varieties positions as Chief Computational Software Development, Senior Manager Product Development and Director Product Development at Ingrain. He has in 2001 Doctorated Munich's University and 2008 Computational Engineering in Fluid Mechanics.

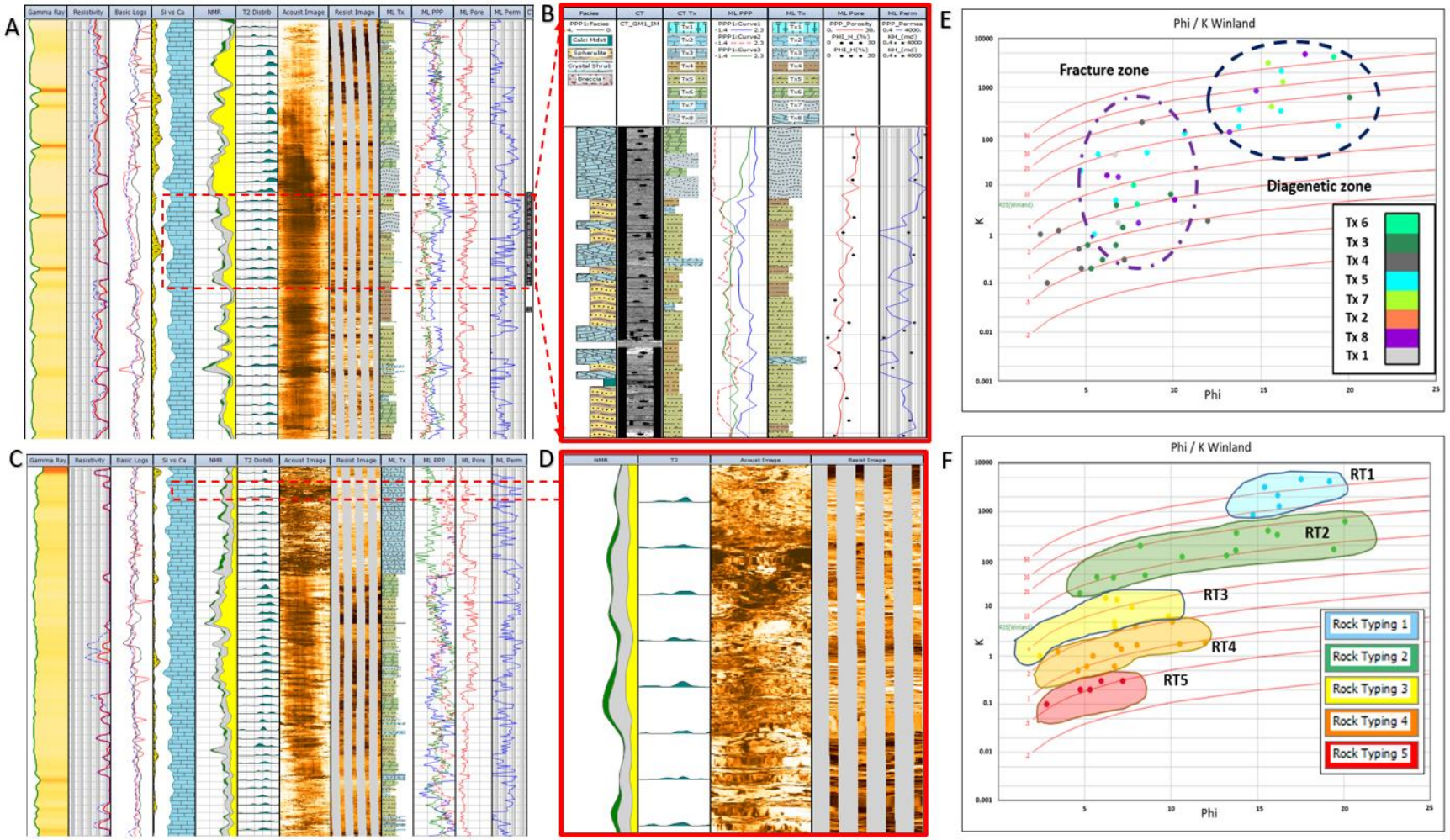

Figure. 8. A- Upper BVF showed textures and properties propagation. B- Zoom showed Core zone. C- Lower BVF showed textures and properties propagation. D- Zoom showed Texture 9. E- Winland R35 Diagenetic zone. F- Rock Typing.

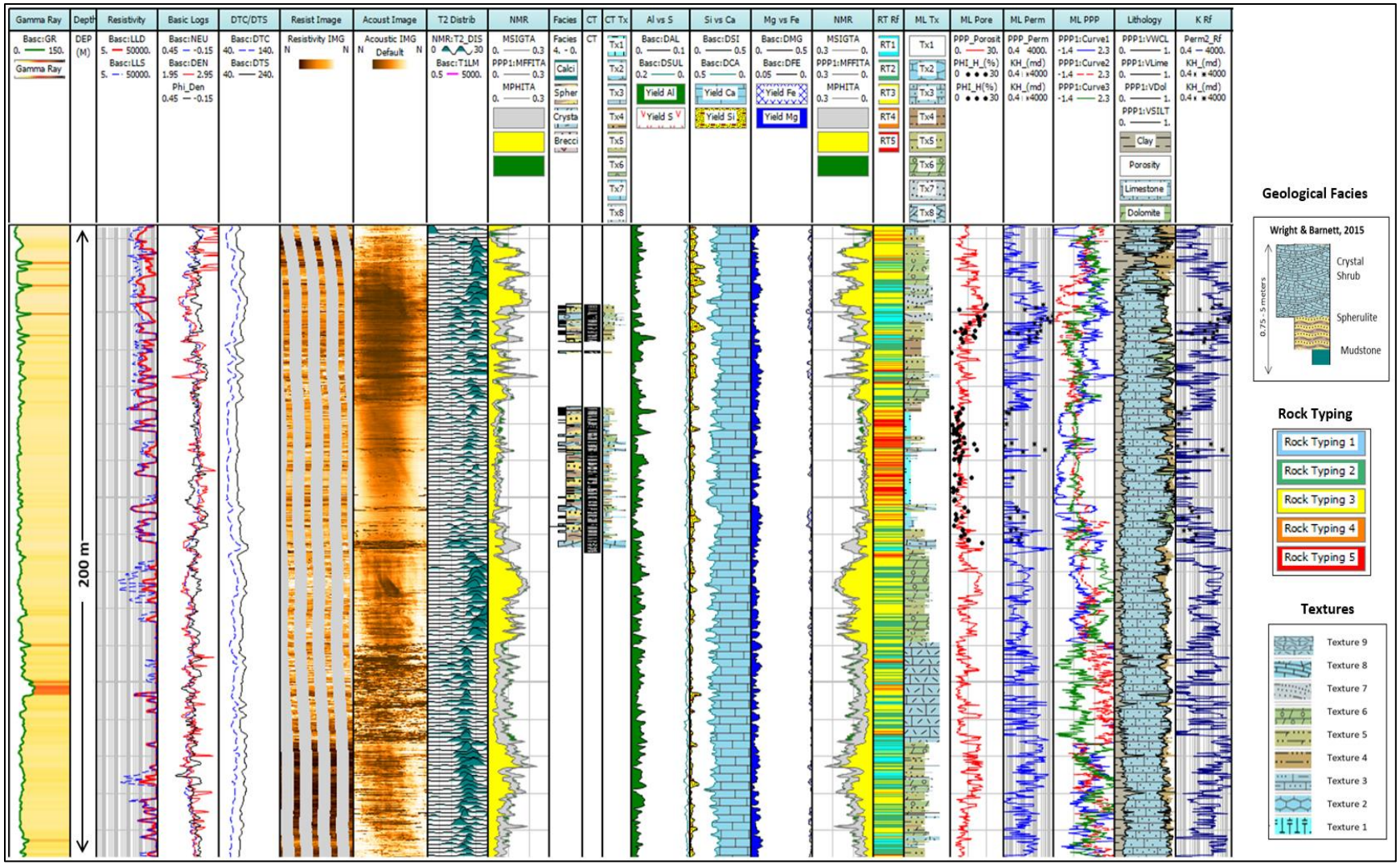

Figure 9. Integrated Plot showed predicted textures, porosity and permeability.